

Article

Design of a Multiple Folded-Beam Disk Resonator with High Quality Factor

Xiaopeng Sun ¹, Xin Zhou ^{1,*}, Lei Yu ², Kaixuan He ², Dingbang Xiao ^{1,*} and Xuezhong Wu ¹

¹ College of Intelligence Science and Technology, National University of Defense Technology, Changsha 410073, China

² East China Institute of Photo-Electronic IC, Bengbu 233042, China

* Correspondence: zhouxin11@nudt.edu.cn (X.Z.); dingbangxiao@nudt.edu.cn (D.X.)

Abstract: This paper proposes a new multiple folded-beam disk resonator whose thermoelastic quality factor is significantly improved by appropriately reducing the beam width and introducing integral-designed lumped masses. The quality factor of the fabricated resonator with (100) single crystal silicon reaches 710 k, proving to be a record in silicon disk resonators. Meanwhile, a small initial frequency split of the order-3 working modes endows the resonator with great potential for microelectromechanical systems (MEMS) gyroscopes application. Moreover, the experimental quality factor of resonators with different beam widths and relevant temperature experiment indicate that the dominating damping mechanism of the multiple folded-beam disk resonator is no longer thermoelastic damping.

Keywords: microelectromechanical systems; quality factor; thermoelastic dissipation; anchor loss; disk resonator



Citation: Sun, X.; Zhou, X.; Yu, L.; He, K.; Xiao, D.; Wu, X. Design of a Multiple Folded-Beam Disk Resonator with High Quality Factor. *Micromachines* **2022**, *13*, 1468. <https://doi.org/10.3390/mi13091468>

Academic Editors: Yusheng Wang and Ha Duong Ngo

Received: 29 July 2022

Accepted: 2 September 2022

Published: 4 September 2022

Publisher's Note: MDPI stays neutral with regard to jurisdictional claims in published maps and institutional affiliations.



Copyright: © 2022 by the authors. Licensee MDPI, Basel, Switzerland. This article is an open access article distributed under the terms and conditions of the Creative Commons Attribution (CC BY) license (<https://creativecommons.org/licenses/by/4.0/>).

1. Introduction

Microelectromechanical disk resonators exhibit tremendous potentials in many transduction applications [1–4], benefitting from their symmetrical structure and mature fabrication process. The mechanical quality factor (Q) of the resonator, which describes the ratio of the totally stored energy to the dissipated energy per vibration cycle, is directly related to the sensitivity and signal-to-noise ratio of the transducer devices. There are different sources of energy dissipation in MEMS resonators, including viscous air damping, thermoelastic damping (TED), anchor loss, surface loss, phonon-phonon scattering, and intrinsic material loss [5,6]. Different kinds of dissipation mechanisms are treated as parallel dampers, and the overall Q is determined by $\sum Q^{-1} = \sum Q_i^{-1}$, where i labels different mechanisms. When air damping is minimized through high vacuum packaging, energy dissipation in most disk resonators is mainly governed by the TED [7,8].

TED is related to the coupling of thermal and elastic deformation fields of the resonator through the coefficient of thermal expansion of the material. Using high-quality non-silicon material is one promising approach but it faces manufacturing challenges [9,10]. Thus, optimizing the structure design of silicon MEMS resonators to improve the quality factor is still attractive due to the mature processing technology. The reported Q -enhancing methods for disk or ring resonators include optimizing the thickness distribution [1], introducing slots [11], adding lumped masses to the flexural body [1,12], and many other topological optimization methods [13–16]. Among them, adding lumped masses to realize stiffness-mass decoupling has an obvious improvement effect. However, the existing arrangement of masses in disk resonators is limited to hanging or attaching to the flexible rings, which is not conducive to improving the effective capacitance area and the upper limit of performance [14]. The radially pleated disk resonator reported in [15] shows great potential in the quality factor even without introducing lumped masses design, which

has advantages in vibration amplitudes over other topological forms such as cobweb and honeycomb, but there is still a lot of room for improvement.

This paper designs a new multiple folded-beam disk resonator, which inherits the advantages of the radially pleated design, and also introduces lumped mass layers with better adaptability to the frame structure. The measured Q after processing reaches 710 k, proving to be a record in flexure silicon disk resonators, showing great potential for MEMS gyroscopes application.

2. Device Design and Modeling

Based on the widely used Zener's standard model of TED [17]

$$Q_{\text{TED}} = \frac{C_v}{E\alpha^2 T_0} \left(\frac{2\pi f_0}{f_Z} + \frac{f_Z}{2\pi f_0} \right) \quad (1)$$

$$f_Z = \frac{\pi^2 \chi}{b^2} \quad (2)$$

where C_v is the heat capacity at constant volume, E is the Young's modulus, α is the linear coefficient of thermal expansion, T_0 is the equilibrium temperature, f_0 is the resonant frequency, and f_Z is the thermal relaxation rate related to the thermal diffusivity χ and the strained beam width b . For most silicon-based MEMS resonators, smaller beam width can increase the thermal relaxation rate and reduce the resonant frequency, thus separate f_0 from f_Z and realize high Q_{TED} . Considering the limitations of processing technology and the requirement of resonator stiffness, b cannot be infinitely reduced, and there will be a lower limit. Then we can introduce lumped masses to further decrease f_0 without affecting f_Z [12]. However, the maximization of this stiffness-mass decoupling effect is usually limited to the non-ideal compatibility between the frame and masses. Directly hanging masses on the outer rings also has a certain impact on the equivalent capacitance area and mechanical sensitivity of the resonator. Here, we propose another design idea. We carry out the integrated design for the multiple folded beams and the lumped mass layers from the beginning to gain great structure coherence. Then we further decrease the beam width and increase the mass width under the premise of ensuring rigidity. This trick can make full use of the stiffness-mass decoupling effect, thus provide lower f_0 and higher f_Z to realize greater Q_{TED} .

The multiple folded-beam disk resonator we designed is shown in Figure 1a. The resonator consists of a central anchor, multiple folded beams extending radially, and outer mass layers hanging between the beams. The inner folded beams with small width (b) can effectively separate resonance frequency and thermal relaxation frequency. With integral design, the outer mass layers help to further increase the effective mass and reduce the resonant frequency. Besides, the structure vibrates approximately parallel at resonance, which is favorable for increasing the equivalent capacitance area. The diameter of the resonator (D) is 6080 μm , the structure height is 100 μm , the anchor diameter (d) is 2420 μm . The thicknesses of outer mass layers (t_m) are 80 μm . The gap between the electrodes and the resonant structure is 10 μm . The connecting-beam width (b), which shows an important impact on Q_{TED} , is designed from 5.5 μm to 7.5 μm . Considering the displacement coupling of in-plane and out-of-plane deformations in (111) silicon, we selected (100) silicon for fabricating and chose the $n = 3$ wine-glass working mode, accordingly. Note that the Young's modulus and Poisson's ratio of (100) silicon is anisotropic, but holding a 90° rotation symmetry. If we rotate the mode shapes of the $\cos 3\theta$ mode clockwise by an angle of 90, the orientations of the mode shapes relative to the Young's modulus curve are exactly the same as those for the $\sin 3\theta$ mode [18–20]. This ensures that the $n = 3$ modes satisfy frequency matching theoretically, but with distinct mode-shape asymmetry. The $n = 3$ mode shapes of the multiple folded-beam disk resonator are shown as Figure 1b, simulated with a density of 2330 kg/m^3 , thermal expansion coefficient of 2.6 ppm/K and the orthotropic stiffness matrix for (100) silicon with three axes at [100], [010], and [001] crystal orientations

at 273 K. The amplitude of radial motion at the peaks along <110> orientation is distinctly different from that of the two symmetrical peaks.

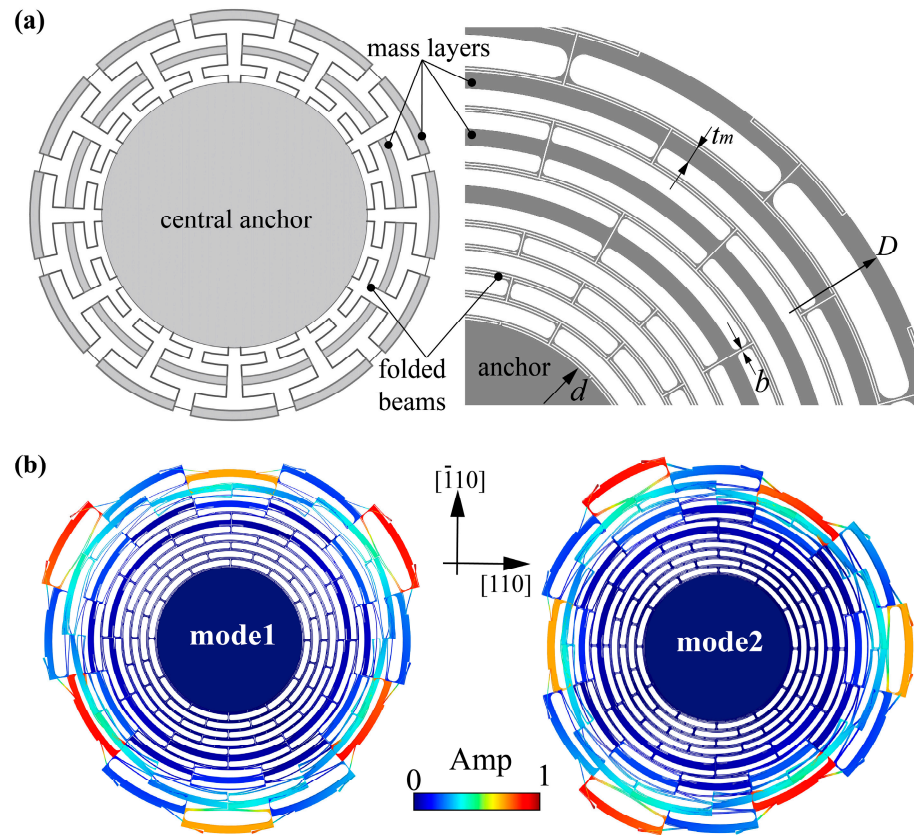


Figure 1. Design of the multiple folded-beam disk resonator. (a) Design concept and structural design of the multiple folded-beam disk resonator. (b) The displacement-normalized mode shapes obtained by simulation.

The dynamical parameters of the proposed multiple folded-beam disk resonator (with a beam width of 6 μm) are calculated and compared with those of a honeycomb disk resonator, which have gone through the comprehensive optimization of structural parameters [16]. The resonant frequency f_0 and thermoelastic quality factor of the working modes are simulated using COMSOL 5.5 with anisotropic (100) silicon. The effective mass m_{eff} and the Coriolis coupling factor κ can be calculated based on the following models [17,18].

$$m_{eff} = \iiint_V \rho(\phi_{X1}^2 + \phi_{Y1}^2 + \phi_{Z1}^2)dV, \tag{3}$$

$$\kappa = \frac{\iiint_V \rho(\phi_{X1}\phi_{Y2} - \phi_{X2}\phi_{Y1})dV}{m_{eff}}, \tag{4}$$

where $(\phi_{Xj}, \phi_{Yj}, \phi_{Zj})$ are the shape functions of the j th ($j = 1, 2$) degenerate modes in geometric coordinates X - Y - Z , and ρ is the density of monocrystalline silicon. The angular gain factor can also be obtained using $A_g = \kappa/n$, where $n = 3$ in this study.

The calculated parameters are summarized in Table 1. Their working frequencies and effect masses compare closely. However, the simulated Q_{TED} of the multiple folded-beam disk resonator is about 2.27 times larger than that of the Honeycomb resonator.

Table 1. Comparison of the simulated parameters of different disk resonators.

Resonator Type	Honeycomb Resonator	Multiple Folded-Beam Disk Resonator
f_0 (Hz)	4150	4231
Q_{TED}	970 k	2.2 million
m_{eff} (mg)	1.75	1.61
A_g	0.84	0.86

The fabrication process of the resonator is shown in Figure 2a. Firstly, etch a substrate silicon-on-insulator (SOI) wafer for 10 μm to form the anchors and generate the thermal oxide layer on it with thermal oxidation technology. Then the substrate and another structure SOI are bonded together through wafer fusion-bonding technology. The handle wafer is moved with chemical and mechanical polishing subsequently. Next, the aluminum wire bonding pads are patterned, and the resonator and the electrodes are formed via deep reactive ion etching (DRIE) technology. Lastly, the device is diced by laser stealth cutting, attached to a chip carrier, wire-bonded and then sealed in a metal shell with a high vacuum of 0.001 Pa. The microscope images of the resonator are shown in Figure 2b.

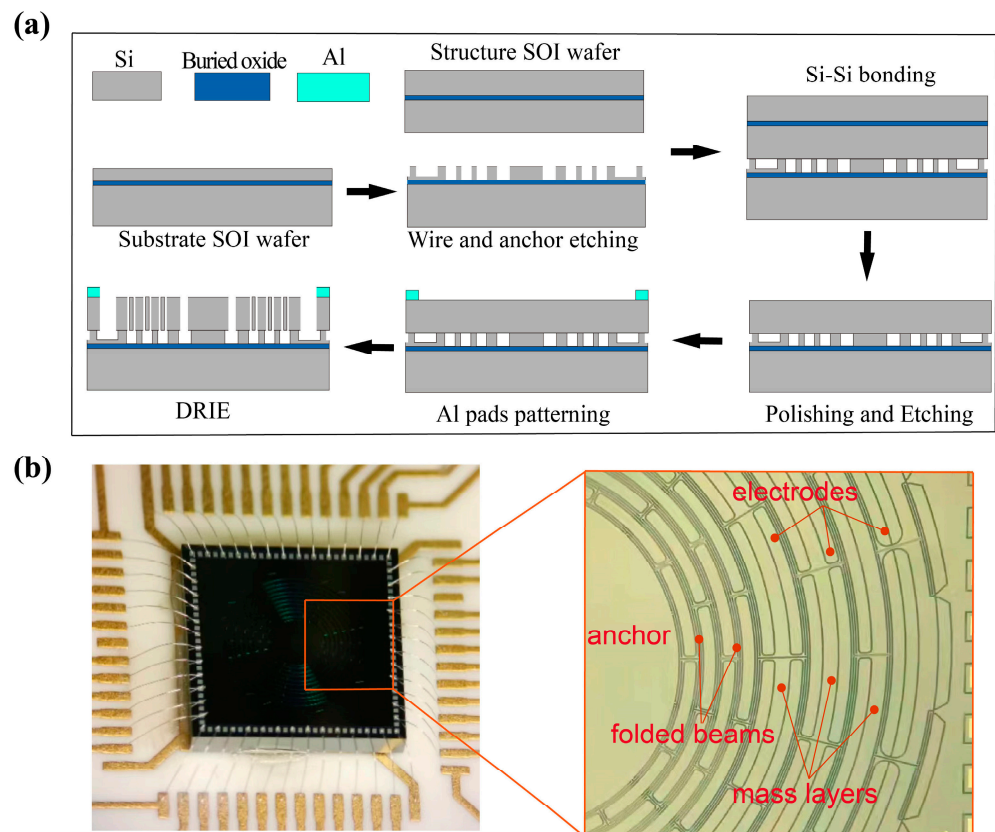


Figure 2. (a) Fabrication processes and (b) Microscope images of the resonator.

3. Resonator Characterization

The resonant frequencies and dissipations of the operational $n = 3$ normal modes of the processed resonator were tested using the setup shown as Figure 3a, among which the double-pole double-throw switch S2 was used to change the testing axis. The frequency responses of the packaged resonator are shown in Figure 3b. Take a resonator with 6 μm -beam-width for example, the initial resonant frequencies of $n = 3$ normal modes are extracted to be $\omega_1 = 2\pi \times 4116.55$ Hz and $\omega_2 = 2\pi \times 4118.24$ Hz, respectively, indicating the initial frequency split is only 1.69 Hz. This shows that the $n = 3$ modes of the (100) silicon resonator hold good frequency-matching characteristics.

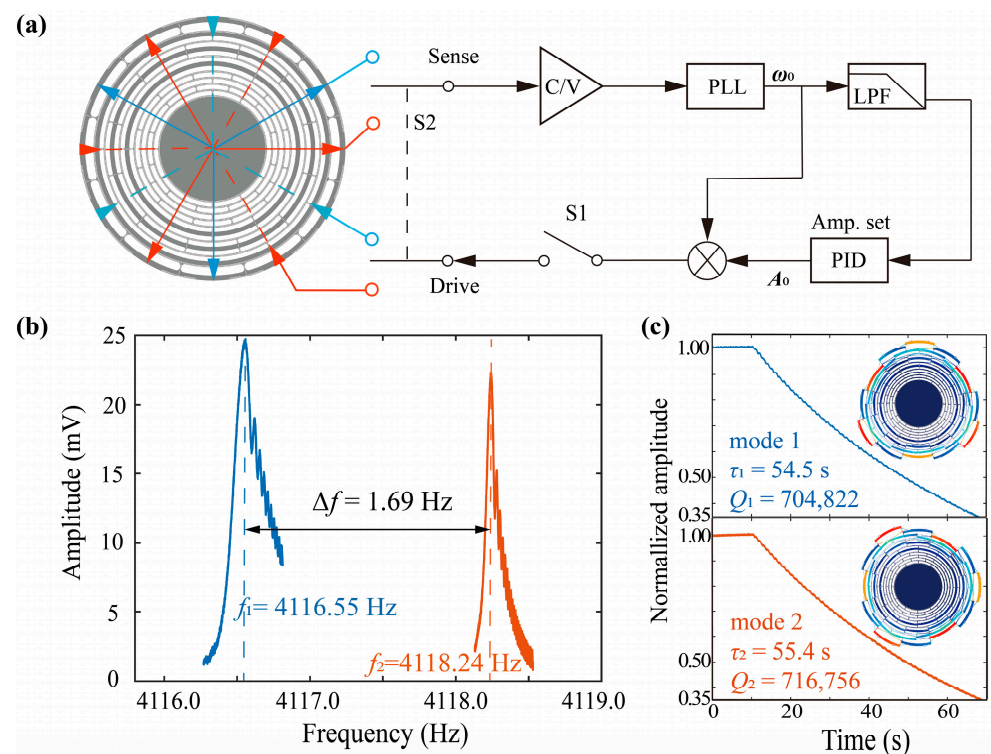


Figure 3. Test system and results. (a) Block diagram of the ring-down test circuit; (b) Frequency sweep curves and (c) Ring-down curves of the driving and sensing modes of the resonator with 6 μm -beam-width.

Then ring-down tests were implemented to characterize the quality factor Q accurately and the decaying time constant τ of the resonator. The resonator was initially actuated at resonance with a constant amplitude using a phase-locked loop (PLL) and a proportion-integration-differentiation (PID) amplitude controller. Then the actuation was stopped by turning off the switch S1. The measured decaying time constants were $\tau_1 = 54.5$ s and $\tau_2 = 55.4$ s, corresponding to $Q_1 = 704$ k and $Q_2 = 716$ k. This proved to be a new record for flexure silicon disk resonators.

4. Results and Discussion

The simulated Q_{TED} and the experimental Q of the fabricated resonators with different beam widths are shown in Figure 4a. With the decrease in beam widths, the simulated Q_{TED} (blue dots) could obviously be elevated, revealing that the Q_{TED} of the 5.5 μm -beam-width was about twice that of the 7.5 μm -beam-width. However, the difference of the measured Q between them was small, violating the distribution of Q_{TED} . Neglecting the air damping in the high-vacuum metallic shell, the experimental quality factor Q of the resonator could be estimated by $1/Q = 1/Q_{\text{TED}} + 1/Q_{\text{other}}$, where Q_{other} was used for calibration which represented the sum of the other damping mechanisms. At room temperature, Q_{other} of resonators with different beam widths was extracted as the red dots in Figure 4a, which was almost constant and ranged from 905 k to 1048 k.

Then we conducted a temperature experiment for the 6 μm resonator whose quality factor was $Q = 716$ k at room temperature. The relation between the quality factor and temperature is shown in Figure 4b. The yellow dots are the measured overall quality factor Q , which increased before the temperature dropped to around -5 $^{\circ}\text{C}$ while gradually decreasing with continuing cooling. The maximal Q is 722 k, close to that measured at normal temperature. Similarly, based on the simulated Q_{TED} (blue dots), we can calculate Q_{other} shown as the red dots in Figure 4b, which changed between 835 k and 1020 k and was almost equal to that in Figure 4a. These results indicated that the dominating damping mechanism is no longer TED.

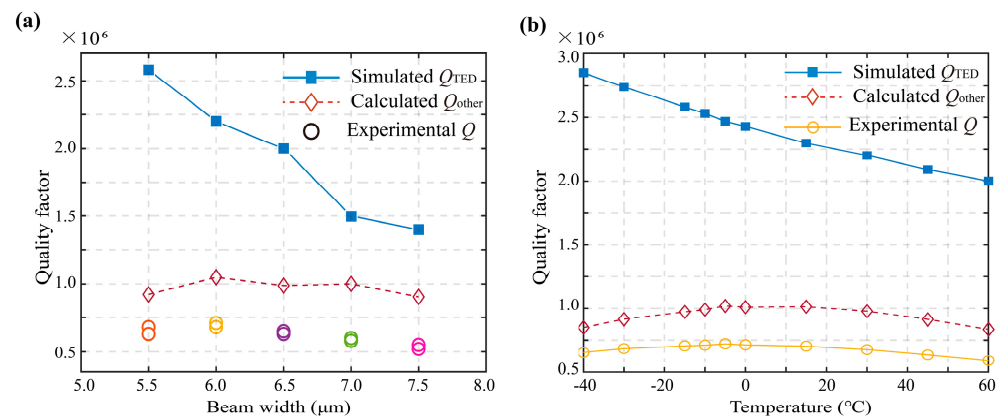


Figure 4. (a) Relation between quality factor and beam width. (b) Relation between quality factor and temperature.

Note that though the (100) silicon for manufacturing was displacement-decoupled in inner and outer plane, the in-plane anisotropy of the material caused distinct modal asymmetry. For $n = 3$ mode of the multiple folded-beam disk resonator shown as Figure 5a, the amplitude of radial motion at the distinct minimal peaks along $\langle 110 \rangle$ orientation was 0.84 relative to that at the two symmetrical peaks, based on the simulated mode shape. Compared to the circumferentially symmetrical vibration in isotropic silicon resonators depicted as Figure 5b, this asymmetry along the circumference may further cause the anchor vibration in $\langle 110 \rangle$ orientation and aggravate support loss [21]. However, unlike the intractable out-of-plane displacement in (111) silicon, the asymmetrical in-plane displacement in (100) silicon resonator may be suppressed, through electrostatic tuning [22,23] or structural compensation [24]. Verification of the above inference is being conducted by us.

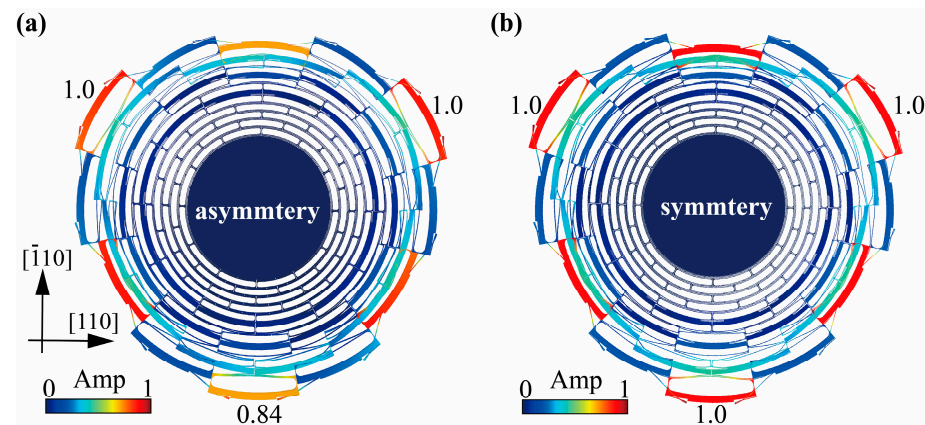


Figure 5. Characterization of the asymmetrical in-plane displacement in (a) (100) silicon resonator owing to the anisotropy of the material and (b) isotropic silicon resonator.

5. Conclusions

In this paper, a multiple folded-beam disk resonator with high Q_{TED} (more than 2 million) was demonstrated. The $n = 3$ modes of the (100) silicon resonator also held good frequency-matching characteristics. The quality factor of the fabricated resonator reached 710 k, proving to be a record in flexure silicon disk resonators. Moreover, conducted temperature experiment indicated that TED is no longer the dominating damping mechanism. As several researches have mentioned, the distinct mode asymmetry of the resonator caused by the in-plane anisotropy of material may lead to anchor vibration and exacerbate the anchor loss to limit the total quality factor. Future study on verifying the inference and compensating the mode asymmetry of this resonator is under way.

Author Contributions: X.Z. and X.S. designed the resonators and conceived the experiments; L.Y. and K.H. fabricated the resonators; D.X. developed the circuits; X.W. and D.X. oversaw and revised this work; X.S. wrote the paper; X.Z. revised the paper; All authors discussed the results and commented on the manuscript. All authors have read and agreed to the published version of the manuscript.

Funding: This research was funded by the National Natural Science Foundation of China (grant number 51905539 and U21A20505), Young Elite Scientist Sponsorship Program by CAST (grant number YESS20200127), and the Natural Science Foundation of Hunan Province for Excellent Young Scientists (grant number 2021JJ20049).

Informed Consent Statement: Informed consent was obtained from all subjects involved in the study.

Acknowledgments: The authors wish to thank Qingsong Li and Peng Wang of National University of Defense Technology for their assistance in device characterization.

Conflicts of Interest: The authors declare no conflict of interest.

References

1. Li, Q.; Xiao, D.; Zhou, X.; Zhuo, M.; Hou, Z.; He, Y.; Wu, X. 0.04 degree-per-hour MEMS disk resonator gyroscope with high-quality factor (510 k) and long decaying time constant (74.9 s). *Microsyst. Nanoeng.* **2018**, *4*, 1–11. [[CrossRef](#)] [[PubMed](#)]
2. Challoner, A.D.; Ge, H.H.; Liu, J.Y. Boeing disc resonator gyroscope. In Proceedings of the 2014 IEEE/ION Position, Location and Navigation Symposium—PLANS 2014, Monterey, CA, USA, 5–8 May 2014; pp. 504–514.
3. Lynch, D.D. Coriolis vibratory gyros. In Proceedings of the Symposium on Gyro Technology, Stuttgart, Germany, 15–16 September 1998; pp. 1.0–1.14.
4. Zotov, S.A.; Trusov, A.A.; Shkel, A.M. High-range angular rate sensor based on mechanical frequency modulation. *J. Microelectromech. Syst.* **2012**, *21*, 398–405. [[CrossRef](#)]
5. Trusov, A.A.; Prikhodko, I.P.; Zotov, S.A.; Shkel, A.M. Low dissipation silicon MEMS tuning fork gyroscopes for rate and whole angle measurements. *IEEE Sens. J.* **2011**, *11*, 2763–2770. [[CrossRef](#)]
6. Weinberg, M.; Candler, R.; Chandorkar, S.; Varsanik, J.; Kenny, T.; Duwel, A. Energy loss in MEMS resonators and the impact on inertial and RF devices. In Proceedings of the Solid-State Sensors, Actuators and Microsystems Conference, Transducers, Denver, CO, USA, 21–25 June 2009; pp. 688–695.
7. Wong, S.J.; Fox, C.H.J.; McWilliam, S.; Fell, C.P.; Eley, R. A preliminary investigation of thermo-elastic damping in silicon rings. *J. Micromech. Microeng.* **2004**, *14*, S108–S113. [[CrossRef](#)]
8. Zener, C. Internal friction in solids. *Proc. Phys. Soc.* **1940**, *52*, 152–166. [[CrossRef](#)]
9. Hamelin, B.; Yang, J.; Daruwalla, A.; Wen, H.; Ayazi, F. Monocrystalline silicon carbide disk resonators on phononic crystals with ultra-low dissipation bulk acoustic wave modes. *Sci. Rep.* **2019**, *9*, 18698. [[CrossRef](#)] [[PubMed](#)]
10. Senkal, D.; Ahamed, M.J.; Ardakani, M.H.A.; Askari, S.; Shkel, A.M. Demonstration of 1 million Q-factor on micro-glass blown wineglass resonators with out-of-plane electrostatic transduction. *J. Microelectromech. Syst.* **2015**, *24*, 29–37. [[CrossRef](#)]
11. Candler, R.N.; Duwel, A.; Varghese, M.; Chandorkar, S.A.; Hopcroft, M.A.; Park, W.-T.; Kim, B.; Yama, G.; Partridge, A.; Lutz, M.; et al. Impact of geometry on thermoelastic dissipation in micromechanical resonant beams. *J. Microelectromech. Syst.* **2006**, *15*, 927–934. [[CrossRef](#)]
12. Zhou, X.; Xiao, D.; Wu, Q.; Hou, Z.; He, K.; Wu, Y. Mitigating thermoelastic dissipation of flexural micromechanical resonators by decoupling resonant frequency from thermal relaxation rate. *Phys. Rev. Appl.* **2017**, *8*, 064033. [[CrossRef](#)]
13. Fan, B.; Guo, S.; Yu, L.; Cheng, M.; Zhou, M.; Hu, W.; Zheng, F.; Xu, D. A novel sixteen-sided cobweb-like disk resonator gyroscope with low as-fabricated frequency split between drive and sense modes. In Proceedings of the 2018 IEEE SENSORS, New Delhi, India, 28–31 October 2018; IEEE: New York, NY, USA, 2018; pp. 1–4.
14. Xu, Y.; Li, Q.; Wang, P.; Zhang, Y.; Zhou, X.; Yu, L.; Wu, X.; Xiao, D. 0.015 Degree-Per-Hour Honeycomb Disk Resonator Gyroscope. *IEEE Sens. J.* **2021**, *21*, 7326–7338.
15. Ren, X.; Zhou, X.; Tao, Y.; Li, Q.; Wu, X.; Xiao, D. Radially Pleated Disk Resonator for Gyroscopic Application. *J. Microelectromech. Syst.* **2021**, *30*, 825–835. [[CrossRef](#)]
16. Cameron, C.P.; Gerrard, D.; Rodriguez, J.; Yang, Y.; Ng, E.; Kenny, T.W. A novel spring disk resonator gyroscope for maximizing Q/F. In *2021 IEEE International Symposium on Inertial Sensors and Systems (INERTIAL)*; IEEE: Piscataway, NJ, USA, 2021; pp. 1–2.
17. Lifshitz, R.; Roukes, M.L. Thermoelastic damping in micro- and nanomechanical systems. *Phys. Rev. B* **2000**, *61*, 5600–5609.
18. Cho, J.Y.; Woo, J.K.; Yan, J.; Peterson, R.L.; Najafi, K. Fused-silica micro birdbath resonator gyroscope (μ -BRG). *J. Microelectromech. Syst.* **2014**, *23*, 66–77. [[CrossRef](#)]
19. Chang, C.-O.; Chang, G.-E.; Chou, C.-S.; Chien, W.-T.C.; Chen, P.-C. In-plane free vibration of a single-crystal silicon ring. *Int. J. Solids Struct.* **2008**, *45*, 6114–61132. [[CrossRef](#)]
20. Hopcroft, M.A.; Nix, W.D.; Kenny, T.W. What is the Young's Modulus of Silicon? *J. Microelectromech. Syst.* **2010**, *19*, 229–238. [[CrossRef](#)]
21. Benvenisty, E.; Elata, D. Frequency Matching of Orthogonal Wineglass Modes in Disk and Ring Resonators Made From (100) Silicon. *IEEE Sens. Lett.* **2019**, *3*, 1–4.

22. Zotov, S.A.; Simon, B.R.; Prikhodko, I.P.; Trusov, A.A.; Shkel, A.M. Quality Factor Maximization Through Dynamic Balancing of Tuning Fork Resonator. *Sens. J. IEEE* **2014**, *14*, 2706–2714. [[CrossRef](#)]
23. Wang, Y.; Lin, Y.W.; Glaze, J.; Vukasin, G.D.; Shin, D.D.; Kwon, H.K.; Heinz, D.B.; Chen, Y.; Gerrard, D.D.; Kenny, T.W.; et al. Quantification of Energy Dissipation Mechanisms in Toroidal Ring Gyroscope. *J. Microelectromech. Syst.* **2021**, *30*, 193–202. [[CrossRef](#)]
24. Shu, Y.; Hirai, Y.; Tsuchiya, T.; Tabata, O. Geometrical compensation of (100) single-crystal silicon mode-matched vibratory ring gyroscope. In *2018 IEEE International Symposium on Inertial Sensors and Systems (INERTIAL)*; IEEE: Piscataway, NJ, USA, 2018; pp. 1–2.